

Supplementary Information: Critical Casimir Forces and Colloidal Phase Transitions in a Near-Critical Solvent : A Simple Model Reveals a Rich Phase Diagram.

John R Edison, Nikos Tasios, and Marjolein Dijkstra*

*Soft Condensed Matter, Utrecht University,
Princetonplein 5, 3584 CC, Utrecht, The Netherlands*

Simone Belli and René van Roij

*Institute for Theoretical Physics, Utrecht University,
Leuvenlaan 4, 3584 CE Utrecht, The Netherlands*

Robert Evans

H.H. Wills Physics Laboratory, University of Bristol, Bristol BS8 1TL, United Kingdom

I. SIMULATION METHODS

Our model is based on that of Rabani *et al.* [1]. We model the colloidal suspension as an incompressible ABC mixture on a 2D square lattice. Colloids C are discretized hard discs (HD) with a radius of R lattice sites that can undergo translational motion on the square lattice. The hard-disc Hamiltonian H_C is zero for non-overlapping configurations, and infinite if any pair of colloids overlap. Every lattice site i has an occupancy number $n_i = 1$ if it is occupied by a colloidal disc, and 0 if it is available for an A or a B solvent molecule. For sites with $n_i = 0$ we associate an occupancy number $s_i = -1$ if the site is occupied by A, and $s_i = 1$ if by B. We consider only nearest neighbour interactions and assign an energy penalty $\epsilon/2 > 0$ for every nearest neighbour AB pair to drive AB demixing at sufficiently low temperatures and an energy gain of $-\alpha\epsilon/2$ with $\alpha \geq 0$ for every BC pair to mimic preferential adsorption of solvent B on the colloid surfaces. The total Hamiltonian thus reads

$$H = H_C + \frac{\epsilon}{4} \sum_{\langle i,j \rangle} (1 - s_i s_j)(1 - n_i)(1 - n_j) - \frac{\alpha\epsilon}{4} \sum_{\langle i,j \rangle} n_i(1 + s_j)(1 - n_j) \quad (1)$$

where the summation runs over the set of distinct nearest neighbour pairs ij , and for every lattice site i , $n_i = 1$ if it is occupied by a colloidal disc, and 0 if it is available for an A or a B

* m.dijkstra1@uu.nl

solvent molecule. For sites with $n_i = 0$ we associate an occupancy number $s_i = -1$ if the site is occupied by A, and $s_i = 1$ if by B.

We performed simulations in an elongated simulation box of 256×512 sites in the fixed $(\eta, \tau, \Delta\mu_s)$ -ensemble. For packing fractions η of hard discs that lie within the binodal curve, two-phase coexistence will be observed in the simulation box. The packing fractions of the coexisting phases can be obtained from the resulting density profiles of the hard discs. In order to determine the G-L coexistence more accurately we treat the colloids grand canonically using the staged-insertion technique [2] in combination with the transition matrix (TM) MC method, see e.g.[2–4].

The length L of the simulation box in all our simulations is at least 4 times the correlation length of the bulk solvent reservoir at the composition $x_c = 0.5$, (the maximum correlation length of the solvent reservoir at a fixed τ). We have also taken care to simulate for time scales much longer than the slowest correlation time in the system. The GC-TMMC simulation results reported in our manuscript are for a system size $L = 256$. A typical GC-TMMC run, to locate one coexistence point for the $L = 256$ system, takes $\simeq 600$ CPU hours. For a few state points we compared the results for two different system sizes, $L = 256$ and $L = 512$, and found the coexisting densities to be the same up to the third decimal place. The $L = 512$ system required $\simeq 5000$ CPU hours to simulate one state point. It is not feasible to perform TMMC simulations in system sizes larger than $L = 512$.

II. MEAN FIELD PHASE DIAGRAM : 3D REPRESENTATION

Within a mean-field approximation we analyzed the Helmholtz free energy associated with the Hamiltonian of our ABC model, which can be decomposed as $F_{MF} = F_C + F_{AB} + U_{BC}$, with (i) the pure-colloid contribution $F_C(\eta, T)$ (ii) the mean-field free energy $F_{AB}(x, \eta, T)$ of the binary AB mixture in the free space in between the colloids (with fractions $1 - x'$ and $x' \equiv x/(1 - \eta)$ of A and B, respectively), and (iii) the average adsorption energy U_{BC} of the B solvent on the colloid surfaces. This yields, up to irrelevant constants,

$$F_{MF}(\eta, T, x) = F_C(\eta, T) + \frac{2\epsilon x(1 - x - \eta)}{(1 - \eta)} + k_B T \left[x \ln \frac{x}{1 - \eta} + (1 - x - \eta) \ln \left(\frac{1 - x - \eta}{1 - \eta} \right) \right] - \frac{Z\alpha\epsilon}{v_c} \frac{x\eta}{1 - \eta} \quad (2)$$

where $Z \simeq 2\pi R$ is the effective colloidal coordination number and where $v_c \simeq \pi R^2$ is the effective volume (area in 2D) of the colloid. For $F_C(\eta, T)$ we employ the hard-disc free energy

from Ref. [5] for the fluid phase, and from Ref. [6] for the solid phase. The phase diagram shown in Fig. S1 is based on $Z\alpha = 32$ and $v_c = 1000$, which do not correspond to values used in our simulation studies. Our objective here is to attempt to understand the topology of the simulation phase diagrams *qualitatively* and investigate the possibility of a lower (metastable) G-L critical point.

In Fig. S1, we plot the resulting phase diagrams for various $\tau > 0$, which reveal a closed-loop immiscibility gap and *two* G-L critical points. We plot three slices of the full phase diagram and the locus of critical points of the ternary mixture. This is shown as the dark green curve in the figure, and it smoothly approaches the critical point of the pure solvent mixture $\tau_c^{MF} = 0.0$ (blue diamond symbol). The locus of critical points indeed continues for $\tau < \tau_c^{MF}$. For clarity, we do not present this. The pale green curve is the projection of the critical line on the $\eta - \tau$ plane. The line of colloidal G-L critical points in our simulations should also behave in a similar manner. Furthermore the mean-field theory predicts that at a fixed temperature, there exists an upper G-L critical point and a lower metastable G-L critical point. On increasing temperature the two critical points approach each other, merge and disappear at a certain temperature. This point is indicated by the olive green diamond symbol in Fig. S1. We also observe coexistence of two crystal phases with the same (hexagonal) symmetry but different lattice spacings, also terminating at a critical point. The *topology* of the mean-field phase diagram and its τ -dependence are remarkably consistent with that obtained from simulations.

III. CORRELATION FUNCTIONS

We define the two-point correlation functions as,

$$g_{\alpha\beta}(\mathbf{r}) = \frac{N}{\langle N_\alpha \rangle \langle N_\beta \rangle} \left\langle \sum_{\{i,j|\mathbf{r}_i-\mathbf{r}_j=\mathbf{r}\}} n_i^\alpha n_j^\beta \right\rangle \quad (3)$$

where n_i^α represents the occupancy of species α at site i , N_α is the total number of sites filled with species α , and $N = \sum_\alpha N_\alpha$, is equal to the lattice size. It is now well-established that in fluid mixtures where all species interact via short range potentials, all structural correlations should decay with the same correlation length [7]. In Fig. S3, we plot the quantity $\log |g_{\alpha\beta}(r) - 1|$, for the pairs BB, BC and CC. It is evident that all correlations do decay with the same correlation length, as expected [7], illustrating that the correlations of all species of our ternary mixture remain coupled.

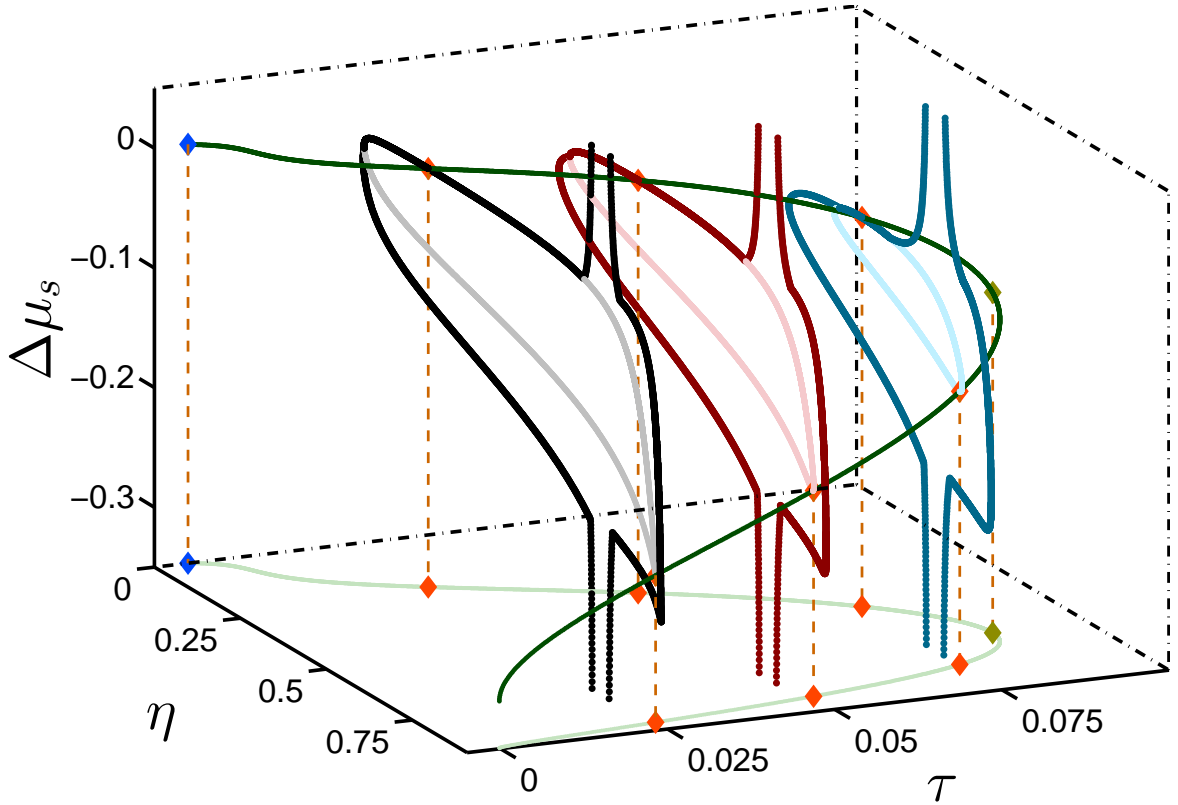


FIG. S1. **Phase behavior of the ternary mixture as predicted by mean-field theory:** Binodals of the ternary colloid solvent system as calculated within mean-field theory plotted in the $\Delta\mu_s$ vs η vs τ representation. We show slices of the full phase diagram for three fixed temperatures $\tau = 0.025$ (black), $\tau = 0.05$ (dark red), and $\tau = 0.075$ (blue). The gray, pale red and pale blue curves correspond to metastable colloidal gas-liquid coexistence, which also terminates at a critical point. The dark green curve is the locus of critical points of the ternary mixture, this approaches smoothly the critical point of the solvent denoted by the blue diamond dot in the limit $\tau \rightarrow \tau_c^{MF} = 0.0$, $\eta = 0$, $\Delta\mu_s = 0$. For each τ we show the upper (stable) and lower (metastable) G-L critical points as indicated by the orange diamond symbols. The olive green diamond symbol corresponds to the point where the upper and lower critical points of the ternary system merge and disappear. The dashed orange lines (guide to the eye) connect the critical points to their projection in the $\eta - \tau$ plane. The projection of the locus of critical points in the $\eta - \tau$ plane is given by the pale green curve.

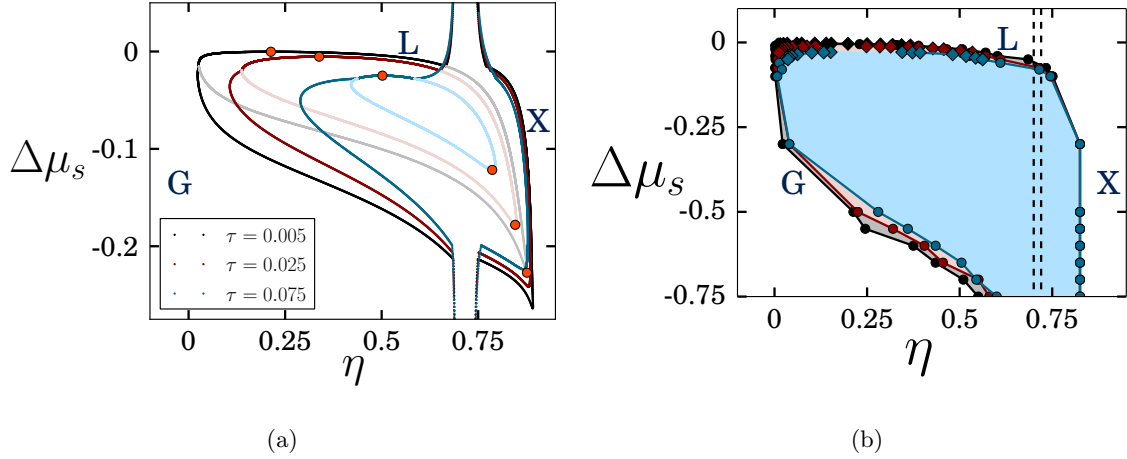


FIG. S2. a) Projections of the binodals of the ternary colloid-solvent system as calculated within mean-field theory for three fixed temperatures $\tau = 0.025$ (black), $\tau = 0.05$ (dark red), and $\tau = 0.075$ (blue) (same as shown in figure S1), on the $\Delta\mu_s - \eta$ plane. b) Phase diagrams of the ABC model computed with simulations for three fixed temperatures $\tau = 0.025$ (black), $\tau = 0.05$ (dark red), and $\tau = 0.075$ (blue) (same as Fig. 3a of our manuscript).

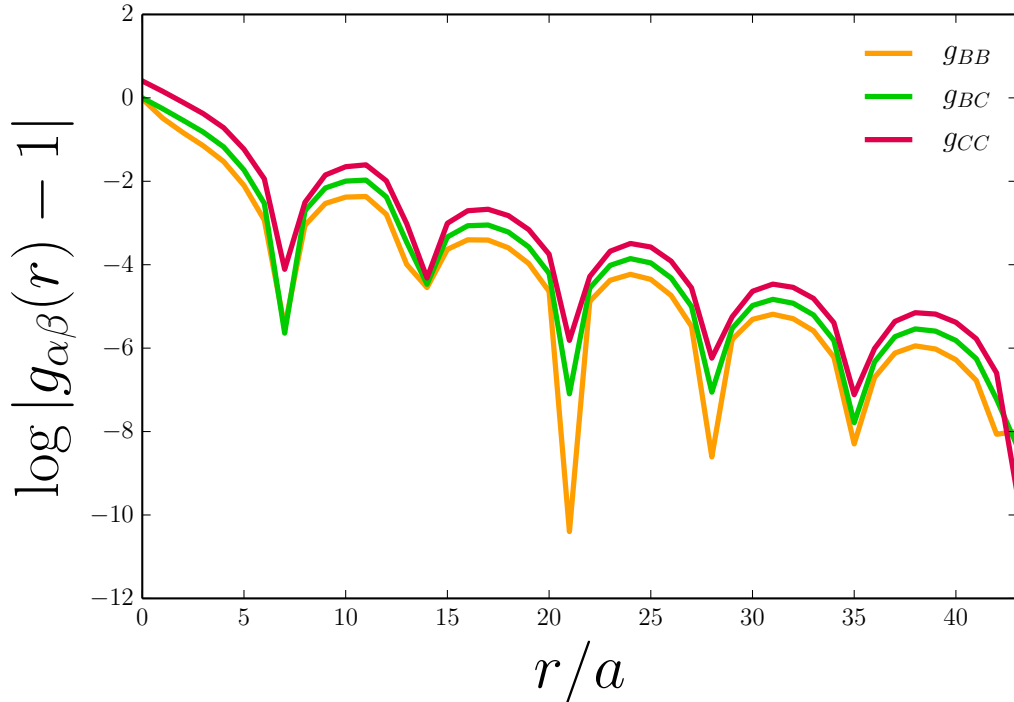


FIG. S3. The partial pair correlation functions plotted as $\log |g_{\alpha\beta}(r) - 1|$ vs distance, normalized by the lattice spacing a , at temperature $\tau = 0.025$, colloid packing fraction $\eta = 0.4$ and chemical potential $\Delta\mu_s = -0.005$. All three correlation functions exhibit the same decay length and period, as predicted by [7].

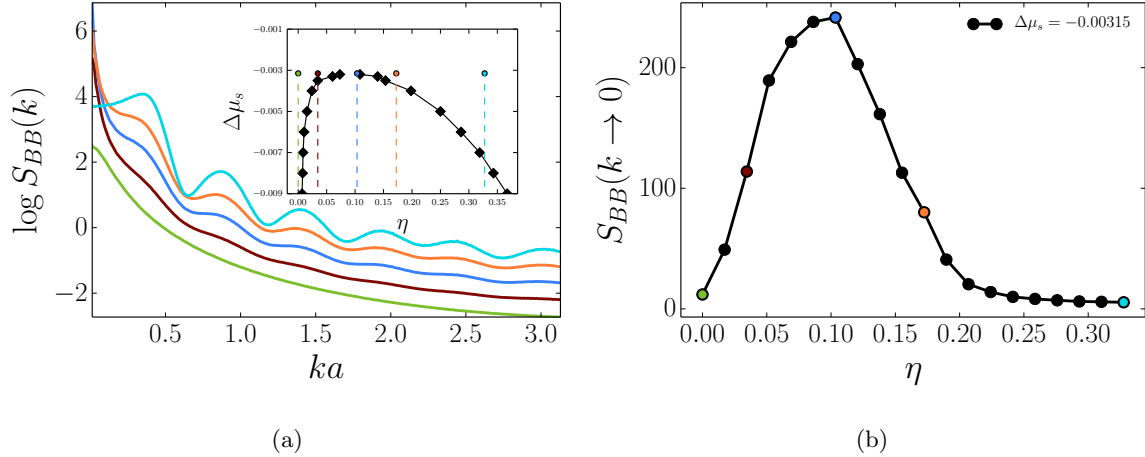


FIG. S4. a) Partial structure factor S_{BB} computed at $\tau = 0.025$, $\Delta\mu_s = -0.00315$, and different values of colloid packing fraction; $\eta = 0.0$ (green), $\eta = 0.0345$ (brown), $\eta = 0.0862$ (blue), $\eta = 0.1724$ (orange) and $\eta = 0.3276$ (cyan). The structure factors, were shifted by 0.5 in log-scale for clarity. The inset shows the G-L binodal for $\tau = 0.025$ (black diamond symbols). b) The maximum value of the structure factor $S_{BB}(k \rightarrow 0)$ vs. the packing fraction η of the colloids.

IV. STRUCTURE FACTORS

At the G-L critical points, whose location can be gleaned from Fig. 3 b) of the paper the solvent-solvent (BB), colloid-colloid (CC) and solvent-colloid (BC) correlations decay with the same, diverging correlation length. Here in figure S4 a) we show the BB structure factor defined as $S_{BB}(k) = (1/N) \langle n_{\mathbf{k}} n_{-\mathbf{k}} \rangle$, where $n_{\mathbf{k}}$, is the Fourier transform of the solvent occupancy profile [8]. We compute $S_{BB}(k)$ at a fixed temperature $\tau = 0.025$, and solvent chemical potential $\Delta\mu_s = -0.00315$, fixed very close to the critical value. We present results at several packing fractions of the colloid η , indicated by dots in the phase diagram, shown in the inset of Fig. S4 a). The long wavelength limits of the partial structure factors $S_{\alpha\beta}(k = 0)$ diverge on approaching the critical point. In Fig. S4 b) we plot the limit $S_{BB}(k = 0)$, obtained from a linear extrapolation of the simulation data, vs η , which shows a maximum corresponding to the state closest to the G-L critical point. Calculations of $S_{BB}(k \rightarrow 0)$ vs η , close to the critical value, can yield a rough estimate of the G-L critical point.

V. EFFECTIVE TWO-BODY INTERACTIONS

The effective two-body interactions were computed by simulating a system of two colloids at fixed $\{\Delta\mu_s, \tau\}$. We fix the position of one colloid at the origin and measure the probability of

finding the other at position $\{x, y\}$. We use the Transition Matrix Monte Carlo technique to make sure the colloids sample the entire range of distances $\{-L_{max} \leq x \leq L_{max}, -H_{max} \leq y \leq H_{max}\}$. The two body potential $U(x, y)$ is obtained as $U(x, y) = -kT \log(P(x, y)/P(\infty, \infty))$.

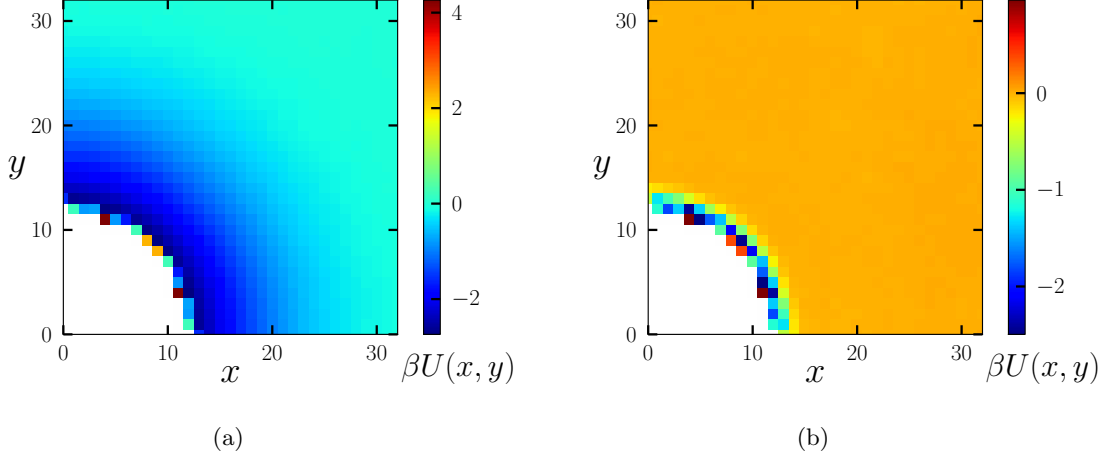


FIG. S5. Effective two body potential between two colloids suspended in a solvent at $\tau = 0.05$ for a) $\Delta\mu_s = -0.01$ and b) $\Delta\mu_s = -0.5$. The area in white is inaccessible due to the hard core repulsion.

The effective colloid-colloid interaction of the discretized colloids (refer to Fig. 1 in paper) in our lattice model is anisotropic; the strength of the interaction close to contact varies substantially. In figure S5 we plot the two-body potential measured at $\Delta\mu_s = -0.01$ and $\Delta\mu_s = -0.5$ at temperature $\tau = 0.05$, where it can be seen that lattice effects are pronounced when the range of the interaction is of the order of 1 – 3 lattice sites. While these lattice effects play no role in G-L coexistence, they play a significant role in G-X coexistence. The crystal phase is facilitated by the colloids aligning along the more energetically favorable directions.

The form of the effective colloid-colloid interaction between our colloidal discs depends on the proximity of the solvent reservoir to its critical point and, to some extent, on the value of the adsorption strength α . In the scaling regime, i.e for small values of $\Delta\mu_s$ and τ , the functional form of these effective interactions is known [9–11] theoretically. In Fig. S6 we plot the effective

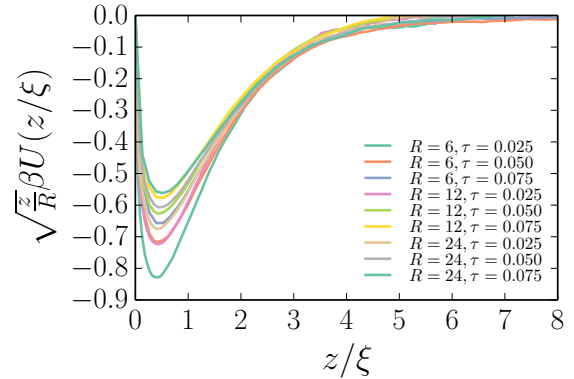


FIG. S6. Effective two-body interactions between a pair of colloids at $\Delta\mu_s = 0$, $\alpha = 19$. ξ is the correlation length of the solvent.

two-body interaction computed at $\Delta\mu_s = 0$ for colloids of different sizes at different temperatures. The distance between the colloids is scaled with the correlation length of the bulk reservoir. Our data shows good scaling behaviour, except at short distances where scaling is no longer applicable and where lattice effects become important. That we find good scaling gives us confidence that our simulations capture correctly the fluctuations responsible for the Casimir attraction.

VI. MOVIE INFORMATION

Movie I (SI-movie-01.mov) shows a ternary ABC mixture with neutral colloids ($R = 6, \alpha = 0, N_c = 64$), with no preference for solvent species A or B, at colloid packing fraction $\eta = 0.11$ and solvent composition $x = (1 - \eta)/2$ (to the right of the dashed line), in equilibrium with a solvent reservoir (left), with composition $x_r = 1/2$, at the same reduced temperature $\tau = 0.005$ and reduced solvent chemical potential difference $\Delta\mu_s = 0$.

Movie II (SI-movie-02.mov) shows a ternary ABC mixture with colloids that strongly prefer solvent species B ($R = 6, \alpha = 19, N_c = 64$), at colloid packing fraction $\eta = 0.11$ (to the right of the dashed line) in equilibrium with a solvent reservoir (left), with composition $x_r = 1/2$, at the same reduced temperature $\tau = 0.005$ and reduced solvent chemical potential difference $\Delta\mu_s = 0$.

Movie III (SI-movie-03.mov) shows a canonical ensemble simulation of a ternary ABC mixture with $N_c = 128$ colloids, in a system of 256×512 lattice sites, at reduced temperature $\tau = 0.05$ and reduced solvent chemical potential difference $\Delta\mu_s = -0.005$ ($R = 6, \alpha = 0.6$). The system exhibits a supercritical colloidal phase.

Movie IV (SI-movie-04.mov) shows a canonical ensemble simulation of a ternary ABC mixture with $N_c = 348$ colloids, in a system of 256×512 lattice sites, at reduced temperature $\tau = 0.05$ and reduced solvent chemical potential difference $\Delta\mu_s = -0.04$ ($R = 6, \alpha = 0.6$). The system exhibits colloidal gas-liquid (G-L) coexistence.

Movie V (SI-movie-05.mov) shows a canonical ensemble simulation of a ternary ABC mixture with $N_c = 580$ colloids, in a system of 256×512 lattice sites, at reduced temperature $\tau = 0.05$ and reduced solvent chemical potential difference $\Delta\mu_s = -0.3$ ($R = 6, \alpha = 0.6$). The system exhibits colloidal gas-crystal (G-X) coexistence.

[1] E. Rabani, D. R. Reichman, P. L. Geissler, and L. E. Brus, Nature **426**, 271 (2003).

- [2] D. J. Ashton and N. B. Wilding, *Mol. Phys.* **109**, 999 (2011).
- [3] J. R. Errington, *Phys. Rev. E* **67**, 012102 (2003).
- [4] F. A. Escobedo, *J. Chem. Phys.* **127**, 174104 (2007).
- [5] A. Santos, M. López de Haro, and S. Bravo Yuste, *J. Chem. Phys.* **103**, 4622 (1995).
- [6] D. A. Young and B. J. Alder, *J. Chem. Phys.* **70**, 473 (1979).
- [7] R. Evans, R. J. F. Leote de Carvalho, J. R. Henderson, and D. C. Hoyle, *J. Chem. Phys.* **100**, 591 (1994).
- [8] J. Hansen and I. McDonald, *Theory of Simple Liquids*, 3rd ed. (Academic Press, 2006).
- [9] M. Zubaszewska, A. Maciolek, and A. Drzewiński, *Phys. Rev. E* **88**, 052129 (2013).
- [10] B. B. Machta, S. L. Veatch, and J. P. Sethna, *Phys. Rev. Lett.* **109**, 138101 (2012).
- [11] T. W. Burkhardt and E. Eisenriegler, *Phys. Rev. Lett.* **74**, 3189 (1995).